International Journal of Advanced Smart Convergence Vol.12 No.4 134-141 (2023)
http://dx.doi.org/10.7236/IJASC.2023.12.4.134

IJASC 23-4-16

Refinement of Ground Truth Data for X-ray Coronary Artery Angiography (CAG) using Active Contour Model

Dongjin Han

Department of Fire Safety, Kyung-Il university, Associate Professor
han@kiu.ac.kr

Youngjoon Park

Department of Radiological Technology, Cheju-Halla University, Assistant Professor
joon740@chu.ac.kr

Abstract

We present a novel method aimed at refining ground truth data through regularization and modification, particularly applicable when working with the original ground truth set. Enhancing the performance of deep neural networks is achieved by applying regularization techniques to the existing ground truth data. In many machine learning tasks requiring pixel-level segmentation sets, accurately delineating objects is vital. However, it proves challenging for thin and elongated objects such as blood vessels in X-ray coronary angiography, often resulting in inconsistent generation of ground truth data. This method involves an analysis of the quality of training set pairs - comprising images and ground truth data - to automatically regulate and modify the boundaries of ground truth segmentation. Employing the active contour model and a recursive ground truth generation approach results in stable and precisely defined boundary contours. Following the regularization and adjustment of the ground truth set, there is a substantial improvement in the performance of deep neural networks.

Keywords: *Ground Truth Improvement; Coronary Artery Angiography; U-Net*

1. Introduction

Is 'ground truth' truly the ultimate truth? The task of ground truth labeling for training data stands as one of the most pivotal aspects of any machine learning system. In the realm of cardiology, X-ray coronary angiography stands as the gold standard for evaluating and identifying coronary artery abnormalities. Yet, detecting blood vessels in coronary angiograms presents an intricate challenge. These angiograms often exhibit non-uniform illumination, weak contrast between arteries and the image background, and occlusion due to various organs or medical devices. Numerous successful methods have been proposed to detect and estimate

Manuscript Received: october. 12, 2023 / Revised: october. 18, 2023 / Accepted: october. 23, 2023
Corresponding Author: han@kiu.ac.kr
Tel: +82-10-9656-3412, Fax: +82-53-600-4020
Author's affiliation (Department of Fire Safety, Kyung-Il university, Associate Professor, Korea)

coronary arteries in X-ray angiography. These methods employ diverse models and filters, specifically designed for identifying elongated objects [1–3]. However, the recent surge in neural network-based technologies has exhibited exceptional performance across various domains of computer vision, including medical image analysis. This surge has led to a rapid influx of works utilizing deep neural network-based methods for coronary artery detection in X-ray angiography [4–8].

Deep learning methods heavily rely on robust ground truth. Recent studies underscore how the performance of deep networks is significantly influenced by the size and quality of the training data. Achieving high performance often hinges on a large number of meticulously annotated training samples, a task demanding substantial human effort. The creation and curation of ground truth for datasets stand as paramount and critical issues in tasks such as recognition, segmentation, and other data-driven methodologies.

Generating high-quality ground truth remains a highly demanding and time-consuming endeavor. Numerous

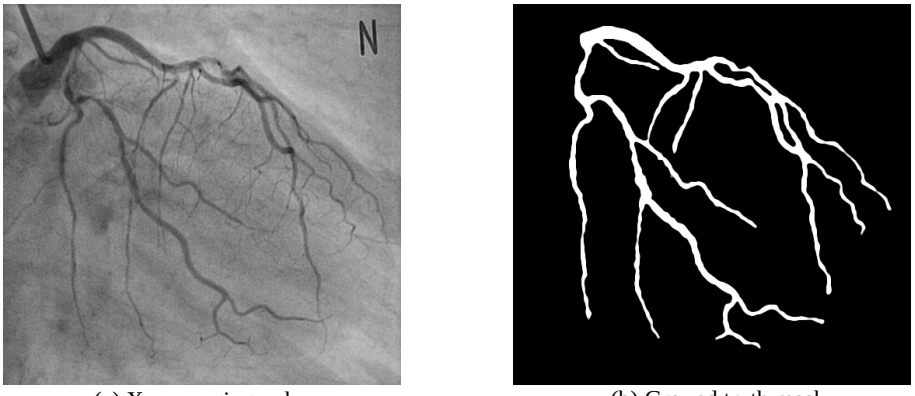

(a) X-ray angiography (b) Ground truth mask

Figure 1. Coronary angiography and its ground-truth mask

researchers and experts invest considerable time and effort in the generation of labeled datasets. Insufficient or flawed ground truth can markedly degrade the performance of devised systems [7]. For precise automatic medical image segmentation, pixel-level annotations play a crucial role. Accurate annotations are pivotal for optimizing the performance of deep networks. However, manual labeling, while essential, poses inherent challenges, notably in dealing with thin and elongated objects like vessels within X-ray coronary angiography (CAG). In Figures 1 and 2, the boundaries of X-ray coronary arteries appear blurry and complex, rendering precise manual annotation more challenging. The inherent difficulty in defining clear and unique boundaries complicates this task. Additionally, manual annotation is inherently subjective, influenced by operator skill, habitual practices, and performance. Operator discretion plays a role, where some vessels might be overlooked due to their perceived lower relevance in disease diagnosis. Medical professionals might prioritize certain coronary arteries over others, leaving some arteries unmarked. Figures 1 and 2 highlight the pruning of numerous small vessels in the original image (a), evident in the mask image (b). While these pruned vessels might not significantly contribute to disease diagnosis or evaluation, their absence can notably affect the consistency and performance of deep networks. The inter-observer variation commonly present in medical image interpretations further complicates matters. Annotation tasks are inherently subjective and subject to operator influence, such as skill, habitual practices, and individual performance. Consequently, some vessels might be overlooked due to their perceived lower relevance in disease diagnosis. Medical professionals might

prioritize certain crucial coronary arteries while leaving other vessels unmarked. The removal of small vessels, as depicted in Figure 2, may not heavily impact disease diagnosis, yet it significantly influences the algorithm's consistency and performance.

The need for refining and modifying ground truth arises from several factors:

1. Blurry vessel boundaries
2. Inaccurate manual segmentation
3. Unmarked objects such as excluded arteries, catheters, and medical equipment
4. Inter-observer variation
5. Alteration of the project's purpose or goal

To address items 1 and 2, subtle modifications and reshaping will be applied to the ground truth. Regarding the third item, high-level knowledge is necessary. For the fourth item, the annotation philosophy for the same data may be reconsidered, or adjustments to the target region could be made. Rather than starting from scratch, if feasible, automatic consistent modifications can be made to existing ground truth data. It's important to note that our proposed method does not fall under the umbrella of 'Data augmentation'. Data augmentation typically involves artificially increasing the size of the training dataset by manipulating existing data. Our method differs from this technique.

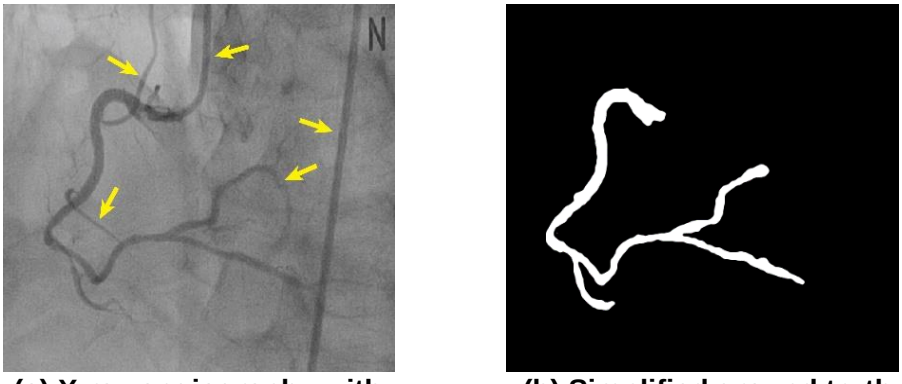

(a) X-ray angiography with **(b) Simplified ground truth**

Figure 2. Omitted arteries and catheter

2. Method

Given ground truth data, which is segmentation masks, the active contour method will modify the ground truth segmentation masks. Active contour model-based contour modification algorithm is very robust and practical one which shows outstanding performance in segmenting enclosed objects. The boundary contour will shrink or expand locally according to image gradient and its constraint. Throughout our experiments, slight modifications are allowed to prevent significant divergence from the original shape of the contour. To enhance accuracy, we employ a recursive method to include smaller vessel branches and artificial objects, such as catheters. This iterative refinement process aims to improve the overall quality of the training ground truth set. Once the entire training ground truth set has been appropriately modified, the deep neural network training will commence.

2. 1 Active Contour Model (Snakes)

The regularization of ground truth masks employs the active contour (snake) method, where the contour evolves over time based on intrinsic geometric measures of the image. This evolutionary process naturally facilitates the splitting and merging of contours, enabling the concurrent detection of multiple objects as well as the delineation of both interior and exterior boundaries. The proposed approach hinges on the correlation between active contours and the computation of geodesics or minimal distance curves. These minimal distance curves exist in a Riemannian space characterized by a metric defined by the content of the image. This geodesic approach for object segmentation allows to connect classical "snakes" based on energy minimization and geometric active contours based on the theory of curve evolution. Formal results concerning existence, uniqueness, stability, and correctness of the evolution were well-proven [9-11]. Given an initial guess for a contour (snake), the energy function of the snake is iteratively minimized using gradient descent minimization. Each iteration takes one step in the negative gradient of the point with controlled step size γ to find local minima. To prevent excessive deviation from the original shape, a constraint term, E_{con}, is introduced. This term serves to enforce adherence to the initially provided shape. The energy function of our snake model is defined as the sum of its continuous external and internal energy function.

$$E^*_{snake} = \int_0^1 E_{snake}\big(V(s)\big)\,ds = \int_0^1 E_{internal}\big(V(s)\big) + E_{external}\big(V(s)\big)ds \quad (1)$$

where $E_{internal}$ and $E_{external}$ represent the internal elastic and curvature energy and external gradient-based energy functions, respectively. Active contour model typically employs elasticity and curvature constraint as internal energy function and edge-based and region-based energy as external. The snake model minimizes a total energy function comprising both internal and external energy terms. It iteratively adjusts the snake's contour by balancing the internal forces that maintain its smoothness and shape against the external forces that guide it towards object boundaries or edges in the image. It can be written again as:

$$E^*_{snake} = \int_0^1 E_{snake}\big(V(s)\big)\,ds = \int_0^1 E_{\text{internal}}\big(V(s)\big) + E_{\text{external}}\big(V(s)\big) + E_{con}\big(V(s)\big)ds \quad (2)$$

E_{con} is introduced. Minimizing the energy function leads to modifications in the original shape. The update function can be represented by the following form:

$$\overline{v_\iota} \leftarrow \overline{v_\iota} + F_{snake}(\overline{v_\iota})$$

where $F_{snake}(\overline{v_\iota})$ is the force on the snake. The update function can be defined by considering the negative gradient of the energy field. This gradient guides the minimization process, facilitating alterations to the original shape.

$$F_{snake}(\overline{v_i}) = -\nabla E_{\text{snake}}(\overline{v_\iota}) = -\big(\omega_{internal}\nabla E_{\text{internal}}(\overline{v_\iota}) + \omega_{external}\nabla E_{\text{external}}(\overline{v_\iota})\big) \quad (3)$$

Assuming the weights α(s) and β(s) are constant with respect to s, this iterative method can be simplified to

$$\overline{v_\iota} \leftarrow \overline{v_\iota} - \gamma\{w_{internal}\left[\alpha\frac{\partial^2\bar{v}}{\partial s^2}(\overline{v_\iota}) + \beta\frac{\partial^4\bar{v}}{\partial s^4}(\overline{v_\iota})\right] + \nabla E_{\text{ext}}(\overline{v_\iota})\} \quad (4)$$

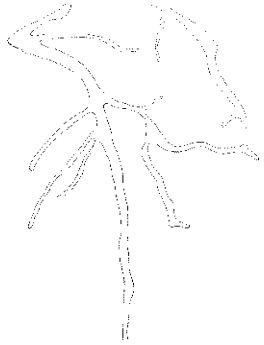

Figure 3. Difference of original and modified masks

(a) Test data **(b) Result** **(c) Original ground truth**

Figure 4. Test Result

In practice, images have finite resolution and can only be integrated over finite time steps. And the step size γ will give us maximum deviation from the original shape of mask contour for each iteration. As the main objective of this work is to refine the original mask for accurate ground truth generation, it is crucial to minimize deviation from the provided ground truth masks. The emphasis lies in maintaining fidelity to the given ground truth masks throughout the modification process. To achieve this, a small value for γ is deliberately chosen.

3. Experiments

The well-known U-net architecture [8] was utilized for vessel segmentation, implemented on an Nvidia DGX-1 server equipped with 8 Tesla V100 GPUs. Our training dataset comprises 147 x-ray coronary artery angiography images, each paired with corresponding labeled data. These labeled data were meticulously generated by expert medical imaging professionals, covering a range of 14 distinct view angles within the dataset. For evaluation, we employed a separate test set obtained from a different patient, consisting of 230 images accompanied by their respective ground truth masks.

Our experimental approach involved the application of the active contour model to refine and delineate vessel boundaries, thereby enhancing the accuracy of the ground truth. The Dice Similarity Coefficient (DSC) score was employed for evaluation. The results notably indicate a significant improvement in vessel detection performance. Specifically, the modified ground truth trained version of U-net demonstrates superior performance compared to the original ground truth trained model.

Following is the detail of the experiments.

The U-net-orig model is trained using the original ground truth mask, generating both train and test data results. These results are represented by Dice Similarity Coefficient (DSC) measurements against both the

original mask (OM) and the mask modified by the active contour method (MM), as depicted in the first row of Table 1. Subsequently, the U-net-mod is trained using MM and provides results for both train and test data, also quantified through DSC measurements. The table demonstrates that the U-net model, when trained with the modified mask (U-net w/ MM), consistently outperforms the model trained with the original mask (U-net w/ OM) across all evaluated scenarios. This improvement is particularly evident in the test results. The Dice Similarity Coefficient (DSC) increases from 0.73 to 0.77 when comparing the performance on the original mask, and from 0.72 to 0.78 on the modified mask. These results indicate that training the U-net model with the modified mask, which is refined using the active contour method, leads to more precise and accurate segmentation of vessels in x-ray coronary artery angiography images.

Table 1. Dice Similarity Coefficient (DSC) Result

	Train vs OM	Test vs OM	Train vs MM	Test vs MM
U-net w/ OM	0.72	0.73	0.69	0.72
U-net w/ MM	0.77	0.76	0.77	0.78

4. Discussion

Our study tackles the challenge of automatically refining ground truth sets specifically for thin and elongated objects such as vessels. However, the tables presented in our paper might be challenging to interpret. Therefore, providing an illustrative example (Fig. 5 and 6) with an explanation could significantly aid comprehension.

For instance, consider the table where the first number in the first row and second column is 0.73. This represents the Dice Similarity Coefficient (DSC) calculated using the conventional U-net model trained on the original mask. Meanwhile, the second row and second column contains the DSC value computed between the original ground truth mask and the output obtained from a U-net model trained using the modified ground truth. Utilizing the active contour model-based algorithm, we modify the mask contours derived from the ground truth set. Our modification strategy ensures that these contours maintain fidelity to the image while staying closely aligned with the original shape. This approach limits substantial alterations from the original segmentation, allowing only minimal changes.

Determining which ground truth mask version (original or modified) better aligns with the actual ground truth presents a challenge. Nevertheless, the noticeable and consistent improvement in the Dice Similarity Coefficient (DSC) displayed in the second column of Table 1 strongly indicates that the modified mask consistently yields superior results. This improvement persists regardless of whether the DSC is measured against the original or modified mask. Figures 5 and 6 present individual Dice Similarity Coefficient (DSC) results for both the train and test datasets.

4. Conclusion

This study presented an innovative approach to refining ground truth data for X-ray Coronary Artery Angiography (CAG) using an active contour model. Our method addresses the key challenges in manual annotation, particularly in accurately delineating blood vessels. This enhanced approach results in more precise and consistent ground truth data, crucial for training effective deep neural networks in medical image analysis.

Experimentally, our method showed substantial improvements in vessel segmentation accuracy. Compared

to traditional manual annotations, the refined ground truth data achieved significantly higher Dice Similarity Coefficient (DSC) scores. This demonstrates the method's efficacy in producing more accurate and reliable datasets for neural network training.

The application of our approach promises to significantly advance the field of medical diagnostics, ensuring higher accuracy in automated image analysis. This advancement could lead to more precise diagnoses and better treatment planning. The potential of this method extends beyond CAG, opening avenues for its application in other medical imaging modalities and integration into clinical workflows. Our findings set the stage for future research in applying computational techniques to enhance healthcare outcomes.

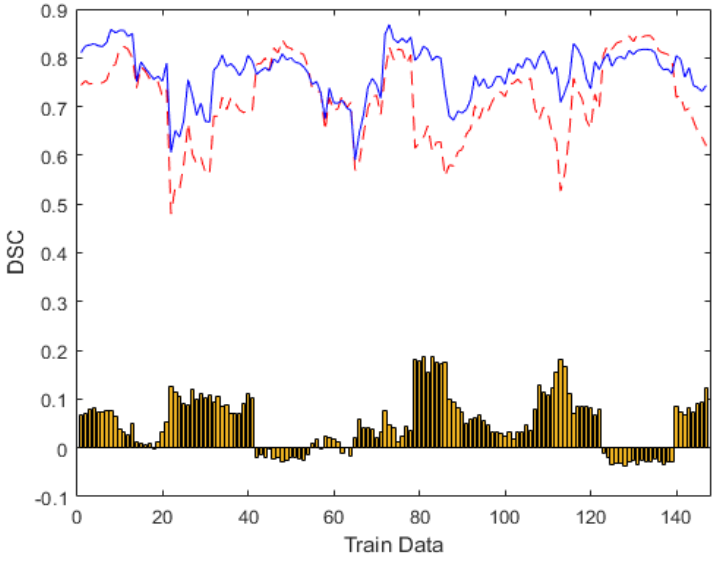

Figure 5. DSC result for test set (147 train data). Blue is DSC result for the network using the proposed method (U-net$_{mod}$). Red is from the network using original masks (U-net$_{orig}$). Bottom bar graph is the subtraction (DSC using U-net$_{mod}$ − DSC using U-net$_{orig}$). The average DSC difference is ≈0.08

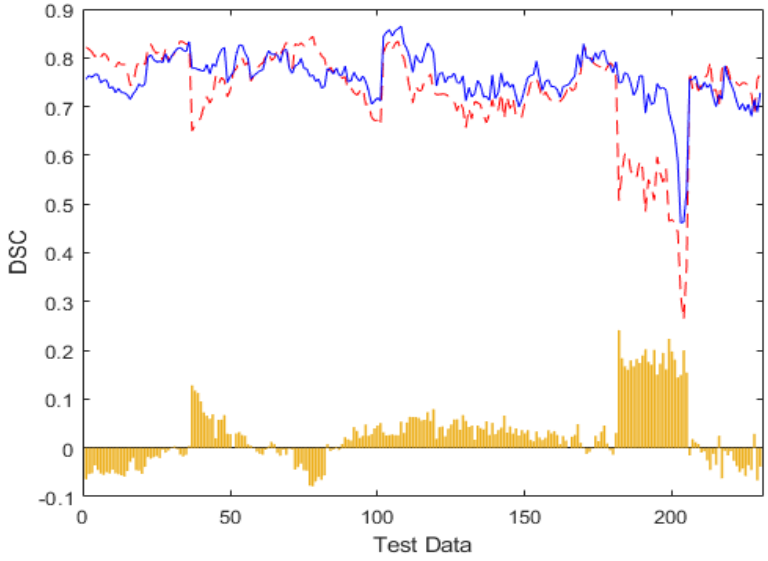

Figure 6. DSC result for test set (230 test data). Blue is DSC result for the network using U-net$_{mod}$. Red is from the network using U-net$_{orig}$. Bottom bar graph is the subtraction (DSC U-net$_{mod}$ − DSC U-net$_{orig}$). The average DSC difference is ≈ 0.06

References

[1] Frangi, A.F.; Niessen, W.J.; Vincken, K.L.; Viergever, M.A. Multiscale vessel enhancement filtering. International conference on medical image computing and computer-assisted intervention. pp. 130–137, Springer, 1998.

[2] Hernandez-Vela, A.; Gatta, C.; Escalera, S.; Igual, L.; Martin-Yuste, V.; Sabate, M.; Radeva, P. Accurate coronary centerline extraction, caliber estimation, and catheter detection in angiographies. IEEE Transactions on Information Technology in Biomedicine 16, pp. 1332–1340, 2012.

[3] Schaap, M.; Metz, C.T.; van Walsum, T.; van der Giessen, A.G.; Weustink, A.C.; Mollet, N.R.; Bauer, C.; Bogunovic´, H.; Castro, C.; Deng, X.; others. Standardized evaluation methodology and reference database for evaluating coronary artery centerline extraction algorithms. Medical image analysis, 13, 701–714, 2009.

[4] Nasr-Esfahani, E.; Samavi, S.; Karimi, N.; Soroushmehr, S.R.; Ward, K.; Jafari, M.H.; Felfeliyan, B.; Nallamothu, B.; Najarian, K. Vessel extraction in X-ray angiograms using deep learning. 2016 38th Annual international conference of the IEEE engineering in medicine and biology society (EMBC). IEEE, 643–646, 2016.

[5] Shin, S.Y.; Lee, S.; Yun, I.D.; Lee, K.M. Deep vessel segmentation by learning graphical connectivity. Medical image analysis, 58, 101556, 2019.

[6] Yang, S.; Kweon, J.; Roh, J.H.; Lee, J.H.; Kang, H.; Park, L.J.; Kim, D.J.; Yang, H.; Hur, J.; Kang, D.Y.; Lee, P.H.; Ahn, J.M.; Kang, S.J.; Park, D.W.; Lee, S.W.; Kim, Y.H.; Lee, C.W.; Park, S.W.; Park, S.J. Deep learning segmentation of major vessels in X-ray coronary angiography. Scientific Reports, 9, 16897, 2019. doi:10.1038/s41598-019-53254-7.

[7] Rennie, C.; Shome, R.; Bekris, K.E.; De Souza, A.F. A dataset for improved rgbd-based object detection and pose estimation for warehouse pick-and-place. IEEE Robotics and Automation Letters, 1, 1179–1185, 2016.

[8] Ronneberger, O.; Fischer, P.; Brox, T. U-net: Convolutional networks for biomedical image segmentation. International Conference on Medical image computing and computer-assisted intervention. Springer, 234–241, 2015.

[9] Kass, M.; Witkin, A.; Terzopoulos, D. Snakes: Active contour models. International journal of computer vision, 1, 321–331, 1988.

[10] Caselles, V.; Kimmel, R.; Sapiro, G. Geodesic active contours. International journal of computer vision, 22, 61–79, 1997.

[11] Chan, T.F.; Vese, L.A. Active contours without edges. IEEE Transactions on image processing, 10, 266–277, 2001.

Sample Availability: Samples of the compounds are available from the authors.